Scanning Tunneling Microscopy Simulations of Nitrogen- and Boron-Doped Graphene and Single-Walled Carbon Nanotubes

Bing Zheng,[†,‡,*] Patrick Hermet,[†,§] and Luc Henrard[†]

[†]Research Center in Physics of Matter and Radiation (PMR), Facultés Universitaires Notre-Dame de la Paix, 61 Rue de Bruxelles, 5000 Namur, Belgium, and [‡]Department of Materials Science, Jilin University, Changchun 130012, China. [§]Current address: University of Liege, B-4000 Sart Tilman Par Liege, Belgium.

ABSTRACT We report on studies of electronic properties and scanning tunneling microscopy (STM) of the most common configurations of nitrogen- or boron-doped graphene and carbon nanotubes using density functional theory. Charge transfer, shift of the Fermi level, and localized electronic states are analyzed as a function of the doping configurations and concentrations. The theoretical STM images show common fingerprints for the same doping type for graphene, and metallic or semiconducting nanotubes. In particular, nitrogen is not imaged in contrast to boron. STM patterns are mainly shaped by local density of states of the carbon atoms close to the defect. STM images are not strongly dependent on the bias voltage when scanning the defect directly. However, the scanning of the defect-free side of the tube displays a perturbation compared to the pristine tube depending on the applied bias.

KEYWORDS: carbon nanotubes · graphene · doping · density functional theory · electronic structures · scanning tunneling microscopy

Tuning the properties of carbon nanotubes (NTs) and few-layer graphene (FLG) by chemical modification represents one of the most promising routes to extend their application possibilities. For example in the quest of cheaper fuel cells, enhanced electrocatalytical properties of aligned N-doped NTs[1] and change in the hydrogen adsorption energy[2] have been reported. Other applications, such as gas sensing, modification of the tube/polymer interface in composite, and protein immobilization, have also been investigated.[3] NT properties can be controlled both by chemical composition (*i.e.*, the amount of doping) and by specific geometry (chirality) of the tubes. The selection of chirality can be only obtained by postproduction tube sorting so far.

Doped NTs[4] and FLGs[5] have been produced in recent years, and the influence of the doping on the morphology of the NTs was highlighted.[6] Electron spectroscopy[7] and X-ray absorption spectroscopy[8] on N-doped samples have revealed that several doping configurations exist, such as substitution (one or more C atom(s) are replaced by N atom(s)) and pyridine-like (three two-coordinated N atoms surround a vacancy site). The presence of N_2 molecules inside the multiwalled NT has also been reported.[8] Simulations have confirmed the stability of N-substitution and N-pyridine-like configurations[4,9] as well as the tendency of N and B atoms to form BN domains when codoping occurs.[10,11] Furthermore, substitution doping of NTs is favored with boron, and it could lead to the formation of BC_3 nanodomains inserted in the 1D-nanotube structure,[12,13] in which the B concentration can be up to 15%.[13] Interestingly, the sp^2 graphitic bonding is not drastically modified by N or B addition. Evidence of a direct relationship between the production method and the atomic configuration is still missing.

Electronic property simulations have shown that N substitution is a *n*-type doping, whereas pyridine configuration is a *p*-type doping for both NTs and FLGs.[4,14] By contrast, B substitution is a *p*-type doping.[15] Electron transport experiments on N-doped NTs present a mixed behavior that could be associated with the presence of *n*- and *p*-type of dopant as expected from the above-mentioned properties of substitution and pyridine-doped configurations.[16] Electron transport calculations also provide valuable information on the electronic transport transparency of BN codoping in NTs,[17] suggesting their possible use as efficient molecular sensors.[14] The unique electronic properties of graphene and its remarkable transport properties have also been reported through the incorporation

*Address correspondence to bing.zheng@fundp.ac.be.

Received for review February 5, 2010 and accepted June 08, 2010.

Published online June 16, 2010.
10.1021/nn1002425

of N or B atoms in substitution within the carbon matrix.[18,19]

Scanning tunneling microscopy (STM) is one among the very few available experimental techniques to investigate the electronic features induced by defects with an atomic resolution. It provides a good insight into the interplay of structural, electronic, and optical properties of materials. Near-field Raman and photoluminiscence experiments have also been proven to give local information of the doping level of the carbon NT network,[20] but with no clear conclusions on the structural aspect so far. Many theoretical and experimental STM studies have been performed to link structural and electronic properties of pure carbon NTs[21−25] and graphene.[26,27] However, STM studies for NTs and graphene with chemical impurities are scarce. Terrones *et al.*[28] and Czerw *et al.*[29] have reported experimental STM images for N-doped carbon NTs, and have observed holes within the carbon structures. They interpreted their STM data and the peak in the density of states (DOS) above the Fermi level obtained by scanning tunneling spectroscopy (STS) as evidence of a pyridine-like site in the NT. Lin *et al.*[30] also reported that protrusions appeared at the defect sites in the STM image of CN_x SWCNTs. BC_3 domains have been reported in B-doped nanotube.[12,31] Besides these, clear STM images that reveal the atomic configurations of N- or B-doped graphene and NTs, from either theoretical or experimental works, are still missing in the literature to the best of our knowledge.

In this article, we report on electronic properties and simulated STM images of N- and B-doped graphene and carbon NTs by using density functional theory calculations. We investigate the STM images of the most probable configurations of chemical modification of graphene and NTs. STM patterns at different bias for N- and B-substitution, and pyridine configurations are analyzed in terms of the local electronic properties. Then, we report the universal STM images for the different doping configurations of sp^2-bonded carbon, independently of the geometry (planar or cylindrical) or the metallicity (metallic or semiconducting NTs). Finally, we investigate the STM images of N- and B-doped carbon NTs in substitution as a function of the dopant concentration.

RESULTS AND DISCUSSION

Doped Graphene: Electronic Structure and STM Images. DOS of pristine and chemically N-doped 2D graphene sheets (substitution and pyridine) are displayed in Figure 1. DOS of pristine graphene is characterized by a linear dependence in energy around the Dirac point (*i.e.*, the energy at which the DOS is zero), and a maximum around ±2.0 eV. For pyridine doping (Figure 1a), localized defect states are mainly located at the Fermi energy (E_F) and at −2.4 eV. Projected density of states (PDOS) on C_N atoms (*i.e.*, C atoms adjacent to N atoms) also displays

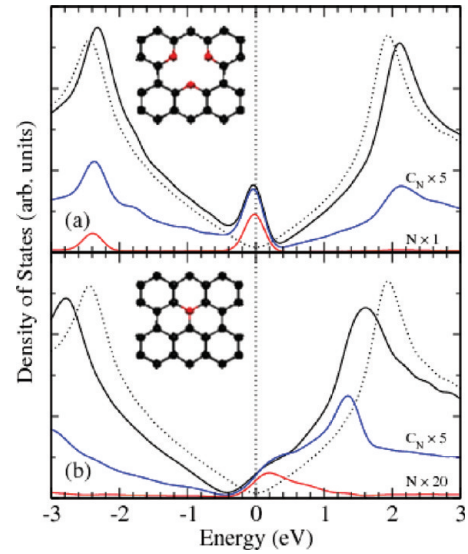

Figure 1. Comparison between DOS of pristine graphene (dashed lines) and N-doped (pyridine (a) and substitution (b)) graphene (solid lines). PDOS on N and C_N atoms is respectively displayed in red and blue solid lines. Note: C_N atoms label C atoms adjacent to N atoms. The Fermi level is set at zero.

a peak at the Fermi level. The Fermi level of pyridine is downshifted by 0.2 eV from that of pure graphene, indicating a *p*-type doping. In the N substitution case (Figure 1b), the Fermi level is upshifted by 0.4 eV from the Dirac point, evidencing a *n*-type doping of the carbon network. Localized defect states are mainly located close to the Fermi level in the conduction band. The peak of the defect states is upshifted by 0.3 eV from that predicted for the pyridine doping. Those results are in agreement with the conclusions by Lherbier *et al.*[18] Using B doping instead of N doping leads to an inverse behavior in the DOS and therefore to a *p*-doped material.[18]

STM image simulations of these doped structures are reported in Figure 2. The maximum height from the tip to the sample surface in our calculations is 3.20 Å, comparable with a typical tunneling distance in an experimental STM procedure[32] (see the definition of the tip−sample distance in the Methods and Computational Details section). We observe that the STM image for the pristine graphene highlights the hexagonal bonding as expected[33,34] (Figure 2a). The STM image for pyridine-doped graphene shows a bright pattern according to the preserved C_3 symmetry of the structure (Figure 2b). This STM image is not very sensitive to the bias sign (the image at a negative bias is not shown) because the localized defect states lie at the Fermi level. The three N atoms (marked as circles on Figure 2b) are not directly imaged whereas the C atoms chemically bonded to the N atoms exhibit an important brightness. In addition, we observe that C_3 symmetric oscillations are evidenced over a region of several hexagons (more than 1 nm). This feature is clearly related to an

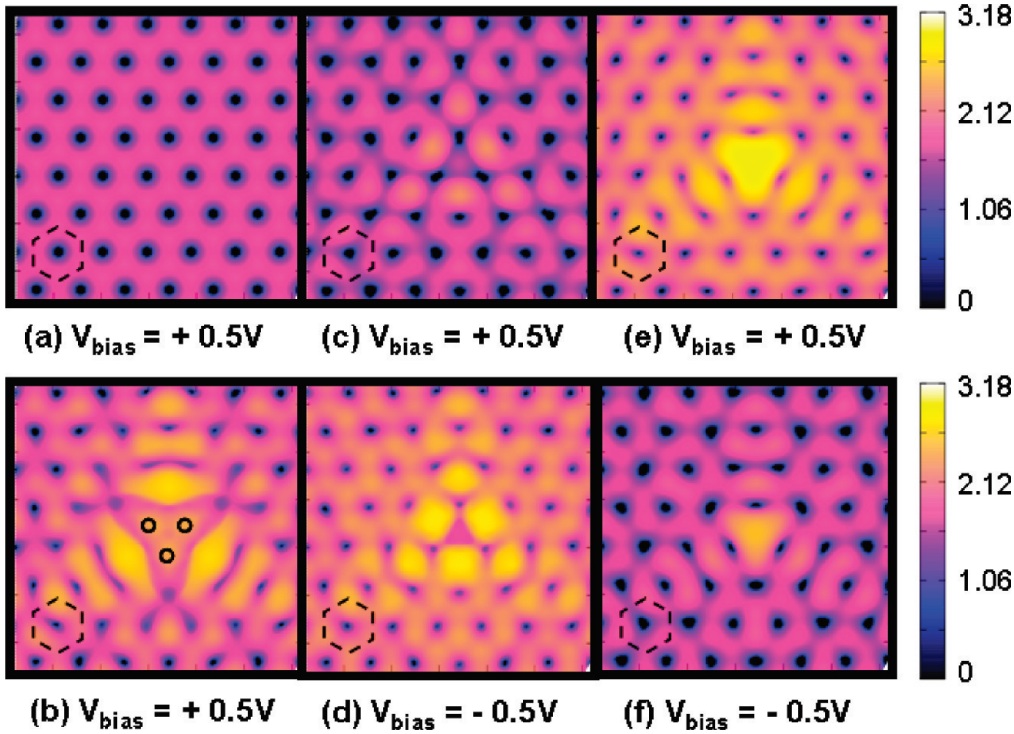

Figure 2. Computed STM images of pristine and doped graphene: (a) pristine, (b) pyridine (locations of 3N are denoted by black circles), (c,d) N substitution, (e,f) B substitution. One dashed hexagon is represented on the different images to highlight the atomic network. The color scales for height are in Å.

electronic effect (as opposed to an atomic displacement) and has been discussed in connection with the electronic transport and mechanical properties of graphitic compounds.[14] Indeed, the fully relaxed system shows that atomic displacements in the direction perpendicular to the graphene plane are below density functional theory (DFT) accuracy, in agreement with previous studies.[18] The STM images of N-substituted graphene show a triangular bright-spot cluster centered on N atom. This similar pattern appears at both positive (Figure 2c) and negative (Figure 2d) bias. However this triangular pattern for negative bias is brighter due to the presence of the electronic states localized on N atoms mainly in the conduction band (see PDOS on N atoms in Figure 1b). Similarly to the pyridine case, this triangular pattern on C_N atoms is related to the extension of wave functions on C atoms neighboring to the dopant.[1,14]

On the contrary, B substitution presents a large, bright triangular pattern centered on the B atom. This pattern is clearly visible for both positive (Figure 2e) and negative (Figure 2f) bias, but it is highlighted for positive bias due to localized B states in the valence band.

The absence of direct imaging of N atoms is explained as followed. In the Tersoff−Hamann approach, the tunneling current is proportional to the local charge density integrated within the $[E_F - eV_{bias};E_F]$ energy range (see eq 1 in Methods and Computational Details section). Figure 3 reports this local density of charge as a function of the *z*-distance between the tip and three characteristic positions: the substituted atom (N or B), the C atom nearest-neighboring to N (C_N) or B (C_B) for substitution or second-nearest-neighboring to N (brightest C atoms) (C_N) for pyridine, and a C atom without interaction with the dopant (C_C). For N-doped configurations, and when *z* is lower than 1 Å, the local charge density (ρ) on N-atoms is more important than the ones on C_N and C_C atoms ($\rho_N(z) > \rho_{C_N}(z) > \rho_C(z)$) (Figure 3a and Figure 3b). This behavior is consistent with the negative charge on the N atoms and the charge transfer to the C_N atoms as previously reported.[1] By contrast, when *z* is larger than 1.5 Å, this behavior is inverted and we have: $\rho_N(z) < \rho_{C_N}(z) < \rho_C(z)$ and $\rho_N(z) < \rho_{C_N}(z) \approx \rho_C(z)$ for substitution and pyridine doping, respectively. Indeed, the electronic transfer from the N atom to the C_N atoms fills the antibonding states of C_N and these antibonding states present a much larger extension than that of the bonding states. As a consequence, the STM images at a distance larger than 1.5 Å mainly image the C_N atoms as shown in Figure 2c and Figure 2d. In the B-substitution case, the charge density on B and C_B atoms are almost equal and much larger than the ones of the C atoms in the network (Figure 3c). Thus, we have an electronic transfer from the carbon network to the B and C_B atoms. The extended antibonding states of B and C_B atoms are occupied, and the STM fingerprint is a large, bright spot centered on the substituted atom.

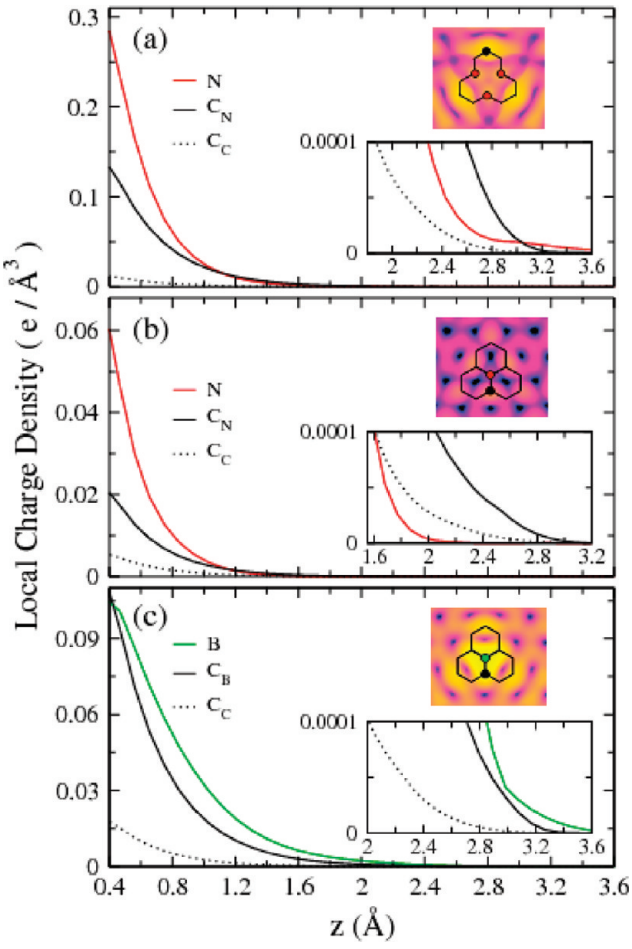

Figure 3. Local charge density as a function of the *z*-distance between the tip and the graphene plane: pyridine (a), N substitution (b), and B substitution (c). Three in-plane positions are considered: the substituted atom (N or B), the C atom adjacent to N or B (C_N or C_B), a C atom unaffected by N or B doping (C_C). Inset: corresponding STM image (zoom of Figure 2 pattern).

Doped Single-Walled Carbon Nanotubes: Electronic Structure. Now, we turn to N- and B-doping effects on electronic structure and STM images of metallic armchair (10,10) and semiconducting zigzag (17,0) NTs. We will show that the very similar fingerprints to those for the planar structures are also observed for the two NT types.

Pristine (10,10) NT is metallic with a 1.5 eV plateau centered at the Fermi level in agreement with experimental measurements (Figure 4a).[24] The Fermi level of N-substituted (10,10) NT shifts toward the conduction band when the dopant concentration (C_d) increases (Figure 4a), suggesting a *n*-type doping for all the concentrations, which is in agreement with experiment.[29] For C_d = 10%, the Fermi energy has shifted by 1.6 eV, in agreement with previous calculation.[29] Such a high doping of homogeneously distributed N substitution has not yet been obtained experimentally in single-walled carbon NTs, whereas it could be locally achieved.[8] We also observe that a gap opens for some doping concentration (for example, around 0.7 eV at C_d = 3%). It is due to the symmetry breaking in the material leading to an anticrossing of the bands (not shown here but studied by Cruz-Silva *et al.*[14]). This gap opening depends more on the symmetry of the dopant positions than on the dopant concentration. Similarly to planar structure, pyridine-doped NT shows a slightly *p*-type doping with a localized defect state at the Fermi level. In addition, its DOS is also much more perturbed at the van Hove singularities (VHS) than for the substitution doping (pyridine doping is similar to a 1%-doping concentration). This is related to the larger perturbations of the sp^2 bonding in the pyridine doping case. Indeed, C−N bond lengths are within 1.40−1.41 Å and 1.33−1.34 Å for N-substitution and pyridine, respectively, whereas C−C bond lengths are 1.42 Å in the pure carbon network.

Pristine (17,0) NT is semiconducting with a predicted band gap of 0.5 eV (Figure 4b). This band gap is underestimated with respect to the experimental one, as reported by previous density functional calculations in the literature.[35] The Fermi energy of N-substituted (17,0) NT shifts further toward the conduction band when C_d increases. N-substituted (17,0) NT is also *n*-type, and shows a metallic behavior for all C_d due to the electronic transfer from the pentavalent N atoms to the carbon network. Strong localized states just above the Fermi level are presented even when C_d is as low as 0.5%. As for metallic (10,10) NT, pyridine-doped (17,0) is *p*-type with a significant defect, centered at the Fermi level, due to N atoms.

Figure 5a and Figure 5b report respectively the DOS of B-substituted (10,10) and (17,0) NTs as a function of the boron concentration. We observe that both B-substituted (10,10) and (17,0) NTs are *p*-type systems. The Fermi energy shifts toward the valence band as C_d increases in agreement with previous conclusions.[12] The C−B bond lengths are within 1.49−1.50 Å slightly longer than the C−C ones in the pure carbon NTs (1.42 Å). By contrast to N-substitution, a very high B-substitution concentration (15%) has been produced by laser ablation technique in single-walled carbon NTs.[13]

Doped Single-Walled Carbon Nanotubes: STM Images. Figure 6 displays the constant current STM images at V_{bias} = ±0.5 V of pristine and doped (10,10) NT. Corresponding STM images for (17,0) are displayed in Figure 7. STM images of pristine (10,10) NT highlight the hexagonal bonding at both positive and negative bias (Figure 6a and Figure 6b), as what is experimentally observed.[25] By contrast, because only the first VHS is included at V_{bias} = 0.5 V, semiconducting (17,0) NT shows C−C bonds parallel to the tube axis slightly more intense than other ones (Figure 7a). The hexagonal bonding is recovered when the first two VHS are included at a larger bias.[25] Similarly to their counterparts in planar structure, a large bright spot is predicted with a C_3 oscillating pattern for pyridine-doped (10,10) NT (Figure 6c and Figure 6d). The bright patterns are due to the contribution of the C atoms neighboring N defect. In addition, we

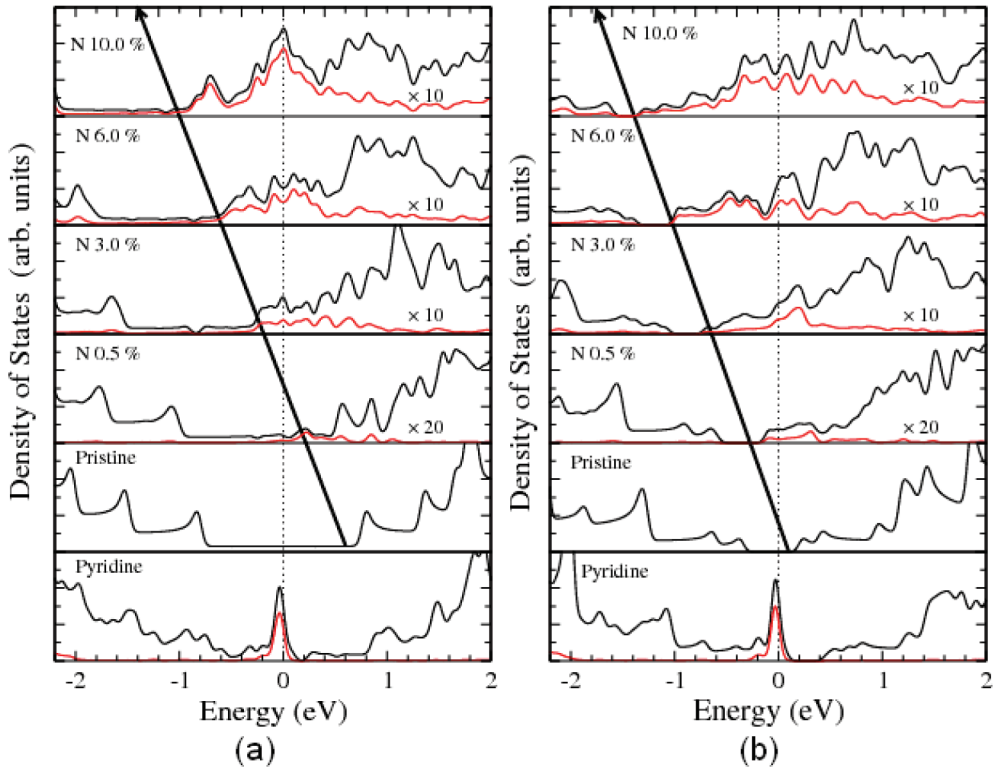

Figure 4. DOS of pristine, pyridine, and N-substituted (a) (10,10) and (b) (17,0) NTs at different concentrations. Black and red lines are total DOS and PDOS on N-atoms, respectively. Arrows are a guide for the eyes indicating the shift of the first VHS. The Fermi level is set at zero.

observe a slightly brighter contrast at the positive bias. We note here that the C−N bond lengths of the relaxed systems are within 1.33−1.34 Å, whereas C−C bond lengths are in the 1.43−1.44 Å range at the vicinity of the N impurities, with respect to 1.42 Å for C−C bonds in the pristine tube. The distortion of the hexagonal network is therefore primarily limited to the first neighbors. At the same time, the N atom in the axial direction moves outward from the nanotube wall by less than 0.2 Å.

The STM images for N-substituted (10,10) NT are very similar to the ones observed in planar structure: a

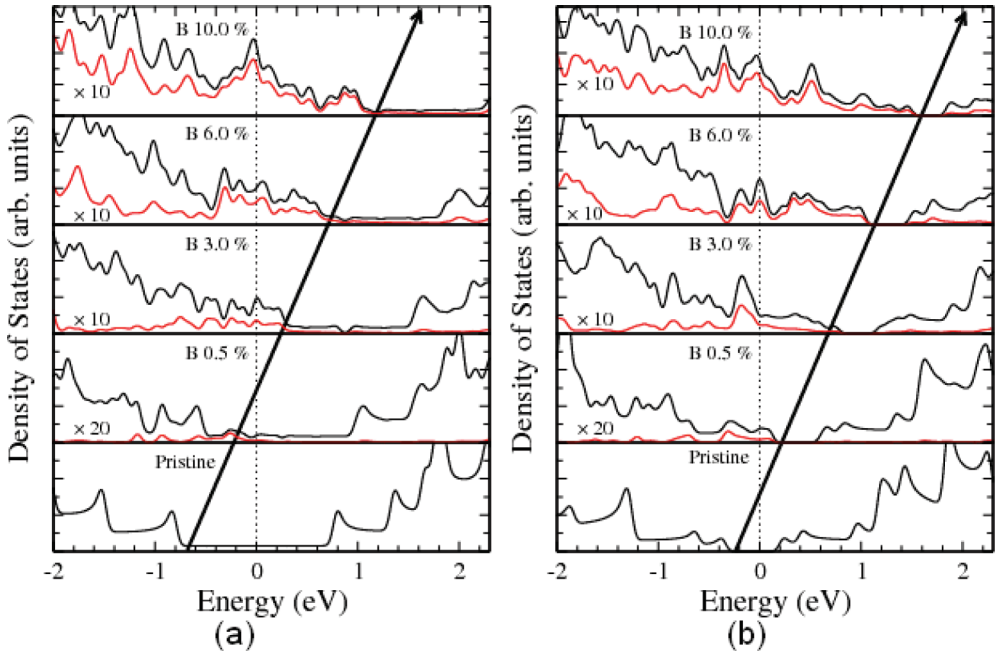

Figure 5. DOS of pristine and B-substituted (a) (10,10) and (b) (17,0) NTs at different concentrations. Black and red lines are total DOS and PDOS on N atoms, respectively. Arrows are a guide for the eyes indicating the shift of the first VHS. The Fermi level is set at zero.

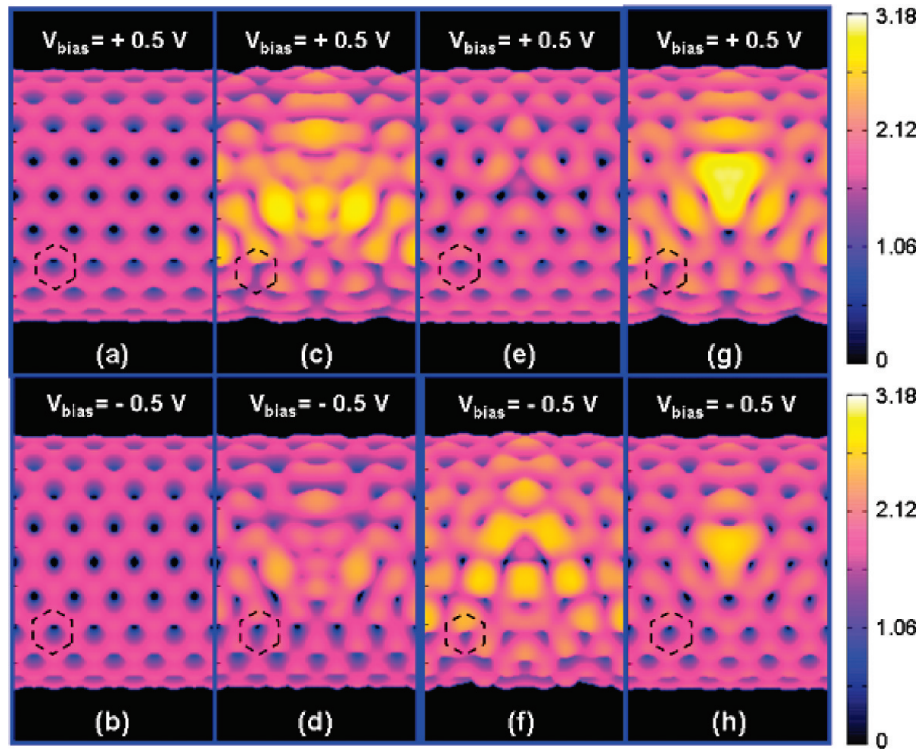

Figure 6. Computed STM images of pristine and doped (10,10) NTs: (a,b) pristine; (c,d) pyridine; (e,f) N substitution; (g,h) B substitution. The horizontal direction is parallel to the nanotube axis. One dashed hexagon is represented on the different images to highlight the atomic network. The color scales for height are in Å.

triangular bright-spot cluster with a dark center at the position of the N atom (Figure 6e and Figure 6f). The charge transfer can also explain that the main STM intensity comes from the C atom surrounding the N defect, C_N, as shown by its PDOS in Figure 4a. When the sign of V_{bias} is changed, the overall triangularly patterned bright spots are shown with less pronounced contrast. As for planar graphene, it is related to the electronic states localized on the C_N atoms that mainly contribute to the DOS above the Fermi level (see Figure 4a). However, as for graphene, the localized states are also presented in the valence band of the doped systems and are imaged under positive bias voltage. The C−N bond lengths in N-substitution doping are within 1.40−1.41 Å, that is, it is very similar to the C−C distance.

The STM image for B-substituted (10,10) NT is a large bright spot centered on the substituted boron and its surrounding carbon atoms (Figure 6g and Figure 6h). Here also when V_{bias} is switched from +0.5 to −0.5 V, as expected, a slight change of contrast is observed. The C−B bond lengths in B-substituted system are within 1.49−1.50 Å. The distortion of the hexagonal network is primarily limited to the first neighbors, but

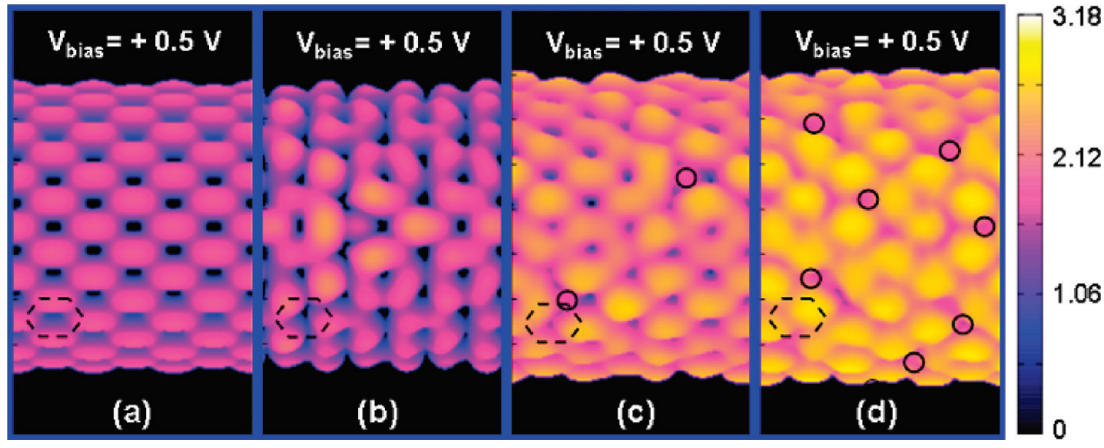

Figure 7. Computed STM images at V_{bias} = +0.5 V of pristine and N-substituted (17,0) carbon NT: (a) pristine; N substitution with doping concentration at (b) 0.5%, (c) 3%, and (d) 10%. The horizontal direction is parallel to the nanotube axis. One dashed hexagon is represented on the different images to highlight the atomic network. The circles show the nitrogen locations in the structure. The color scales for height are in Å.

it is larger than that for the N-substitution. The B atom moves outward from the nanotube wall by less than 0.2 Å.

As an example of the effect of doping concentration, Figure 7 reports the STM simulation of the N substitution of (17,0) NT for several dopant concentrations. As for (10,10) NT, isolated defects present a triangular pattern surrounding a dark point, centered on the N atom but rotated due to the zigzag chirality (Figure 7b). Other studied configurations (B-substitution and pyridine) also show very similar images for semiconducting NTs as those for their corresponding metallic ones (not shown). This overall similarity of the STM fingerprints of graphene, metallic, and semiconducting NTs were not obvious in view of the different electronic properties of the pristine materials.

As C_d increases, interference between originally isolated STM patterns occurs. When C_d is up to be 10% the STM image becomes an ensemble of bright spots. We remind here that, for an isolated defect, the C_N atoms are mainly imaged. Here almost all C atoms are C_N atoms and contribute to the bright area, in contrast to the dark N atoms. We note here that the simulated pattern of N substitution for the high C_d is very similar to the STM image reported by Terrones *et al.*[28] and Czerw *et al.*[29] The pyridine defect shows a more disturbed feature, and experimental STM could also be due to substitutional N, in contradiction with the original interpretation.

Finally, Figure 8 displays the STM images of N and B substitution of (10,10) NT scanning from the defect-free side of the tubes. For N substitution, the STM image is not affected by the N defect at $V_{bias} = +0.5$ V, whereas it is largely affected at $V_{bias} = -0.5$ V. This observation is related to the fact that N states are more localized in the unoccupied states. The valence band DOS of C atoms far from the defect (C_C) is then almost unaffected by the substitution where conduction band DOS is significantly perturbed by N (Figure 4a). For B substitution, the back-side STM images are only significantly affected by B when V_{bias} is positive since DOS of the C_C atoms is mainly disturbed in the conduction band as shown in Figure 5a. We obtain the same conclusions for the semiconducting (17,0) NT (not shown here). These simulations of the defect-free sides open new possibilities to analyze the presence of doping even when the STM tip does not directly scan the defect.

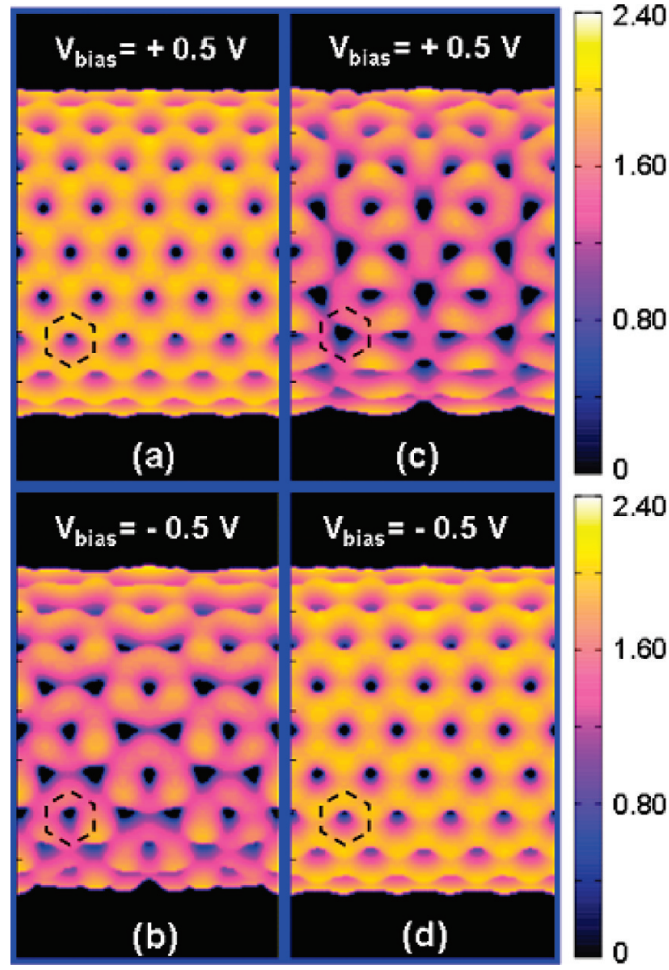

Figure 8. Computed STM images of N- and B-doped (10,10) NT in substitution scanning from the defect-free side of the tube. (a,b) N substitution, (c,d) B substitution. The color scales for height are in Å.

CONCLUSIONS

We have investigated the electronic properties and predicted the STM images of doped graphene and carbon NTs in the pyridine and substitution configurations. This study shows that the Fermi level of N- or B-doped carbon NTs shifts when C_d increases in the 0.5% to 10.0% range. For semiconducting (17,0) NT all doped configurations are metallic, even when the doping concentration is only 0.5%. For pyridine-doped graphene and carbon NTs, the STM fingerprints are bright-spot clusters highlighting the C_3 symmetry of the structure. For N-doped graphene and carbon NTs in substitution, the STM fingerprints are bright-spot clusters in triangular patterns, whereas the fingerprints are large bright spots in the case of B substitution. The sign and magnitude of bias voltage do not influence the features of STM images for either N- or B-doped graphene and NTs. In addition, we have highlighted the importance of the charge transfer from doping defects to their neighboring C atoms to interpret the STM patterns. Finally, the effect of the bias voltage has been demonstrated to be weak on the STM pattern when the defect is directly imaged, but noticeably modifies the STM image far from the defect (back side of the tube). The substrate effects have been neglected in the present approach. A charge transfer could occur between substrate (*e.g.*, "Au") and the carbon systems and this could, in principle, modify the STM image. The stability of the STM pattern with bias voltage in our numerical study is however an indication that the present conclusions hold true for moderate charge transfer from the substrate

to the carbon systems. This work provides a solid theoretical support for future experimental investigations on chemically modified NT carbon nanosystems using STM.

METHODS AND COMPUTATIONAL DETAILS

Density functional calculations were performed with the SIESTA package.[36] Exchange-correlation effects were handled within local density approximation (LDA) as proposed by Perdew and Zunger.[37] Core electrons were replaced by nonlocal norm-conserving pseudopotentials.[38] The valence electrons were described by localized pseudoatomic orbitals with a double-ζ basis set.[39] A hexagonal supercell containing 200 atoms was used for graphene, whereas NTs were placed into tetragonal supercells containing 200 atoms for (10,10) NT and 204 atoms for (17,0) NT. Graphene layers and neighboring NTs were separated by 10 Å vacuum. The first Brillouin zone (BZ) was sampled according to the Monkhorst−Pack scheme.[40] We have used 24 and 41 irreducible *k*-points for graphene and NTs, respectively. Atomic positions for each system were relaxed at fixed lattice parameters using a conjugate gradient scheme until the maximum residual forces on each atom were smaller than 0.007 eV/Å. Real space integration was performed on a regular grid corresponding to a plane-wave cutoff around 300 Ry, for which the structural relaxations were fully converged.

STM topological images were calculated according to Tersoff and Hamann approximation.[41] In this approximation, applying a small bias voltage, V_{bias}, between the tip and the sample yields a tunneling current whose density is proportional to ρ_{STM}:

$$\rho_{STM}(\vec{r}, V_{bias}) = \int_{E_F - eV_{bias}}^{E_F} \sum_{i}^{levels} \sum_{\vec{k} \in BZ} |\varphi_{i,\vec{k}}(\vec{r})|^2 \delta(E_{i,\vec{k}} - E)\, dE \quad (1)$$

where $\varphi_{i,\vec{k}}$ is the wave function whose associated E_i eigenvalues belong to the energy range defined by the integral. When V_{bias} is positive (respectively negative), it provides information of electron density for the occupied (respectively unoccupied) states. We simulated the STM images in constant current (CC) mode according to standard experimental procedures. For a cylindrical system, we have replaced the absolute vertical displacement of the tip by the height of the tip above a circular profile to improve the contrast of surface topography of NTs.[21] In the present work, we defined the tip−sample distance (or tip height) as the distance between the atomic plane and the point $\vec{r}$ (see eq 1). We emphasized that the tip shape and its electronic structure were not taken into account. Consequently, the tip−sample distance could not be directly compared with the experimental value. However, the main effect of the tip−sample distance variation was caught by the present approach. NTs were considered as being self-supported in our calculations.

Acknowledgment. This work is supported by the BNC-TUBE STREP EU project (Project Number 033350). Calculations have been performed at the Interuniversity Scientific Computing Facility (Facultés Universitaires Notre-Dame de la Paix, Namur, Belgium) supported by FRS-FNRS under convention No. 2.4617.07. The authors thank H. Lin, J. Lagoute, A. Loiseau, and V. Meunier for helpful discussions. L. H. is supported by FRS-FNRS.

REFERENCES AND NOTES

1. Gong, K.; Du, F.; Xia, Z.; Durstock, M.; Dai, L. Nitrogen-Doped Carbon Nanotube Arrays with High Electrocatalytic Activity for Oxygen Reduction. *Science* **2009**, *323*, 760–764.
2. Zhou, Z.; Gao, X.; Yan, J.; Song, D. Doping Effects of B and N on Hydrogen Adsorption in Single-Walled Carbon Nanotubes through Density Functional Calculations. *Carbon* **2006**, *44*, 939–947.
3. Terrones, M.; Souza, A.; Rao, A. Doped Carbon Nanotubes: Synthesis, Characterization, and Applications. In *Carbon Nanotubes*; Jorio, A., Dresselhaus, G., Dresselhaus, M., Eds.; Springer: New York, 2008; Vol. 111.
4. Ewels, C. P.; Glerup, M. Nitrogen Doping in Carbon Nanotubes. *J. Nanosci. Nanotechnol.* **2005**, *5*, 1345–1363.
5. Wei, D.; Liu, Y.; Wang, Y.; Zhang, H.; Huang, L.; Yu, G. Synthesis of N-Doped Graphene by Chemical Vapor Deposition and Its Electrical Properties. *Nano Lett.* **2009**, *9*, 1752–1758.
6. Sumpter, B. G.; Meunier, V.; Romo-Herrera, J. M.; Cruz-Silva, E.; Cullen, D. A.; Terrones, H.; Smith, D. J.; Terrones, M. Nitrogen-Mediated Carbon Nanotube Growth: Diameter Reduction, Metallicity, Bundle Dispersability, and Bamboo-like Structure Formation. *ACS Nano* **2007**, *1*, 369–375.
7. Enouz, S.; Stéphan, O.; Cochon, J.-L.; Colliex, C.; Loiseau, A. C-BN Patterned Single-Walled Nanotubes Synthesized by Laser Vaporization. *Nano Lett.* **2007**, *7*, 1856–1862.
8. Enouz, S.; Bantignies, J. L.; Babaa, M. R.; Alvarez, L.; Parent, P.; Le Normand, F.; Stephan, O.; Poncharal, P.; Loiseau, A.; Doyle, B. P. Spectroscopic Study of Nitrogen Doping of Multiwalled Carbon Nanotubes. *J. Nanosci. Nanotechnol.* **2007**, *7*, 3524–3527.
9. Kudashov, A. G.; Okotrub, A. V.; Bulusheva, L. G.; Asanov, I. P.; Yu, V. Shubin; Yudanov, N. F.; Yudanova, L. I.; Danilovich, V. S.; Abrosimov, O. G. Influence of Ni−Co Catalyst Composition on Nitrogen Content in Carbon Nanotubes. *J. Phys. Chem. B* **2004**, *108*, 9048–9053.
10. Ivanovskaya, V. V.; Zobelli, A.; Stéphan, O.; Briddon, P. R.; Colliex, C. BN Domains Included into Carbon Nanotubes: Role of Interface. *J. Phys. Chem. C* **2009**, *113*, 16603–16609.
11. Blase, X.; Charlier, J.-C.; De Vita, A.; Car, R. Theory of Composite $B_xC_yN_z$ Nanotube Heterojunctions. *Appl. Phys. Lett.* **1997**, *70*, 197.
12. Carroll, D. L.; Redlich, P.; Blase, X.; Charlier, J.-C.; Curran, S.; Ajayan, P. M.; Roth, S.; Rhle, M. Effects of Nanodomain Formation on the Electronic Structure of Doped Carbon Nanotubes. *Phys. Rev. Lett.* **1998**, *81*, 2332–2335.
13. Fuentes, G. G.; Borowiak-Palen, E.; Knupfer, M.; Pichler, T.; Fink, J.; Wirtz, L.; Rubio, A. Formation and Electronic Properties of BC_3 Single-Wall Nanotubes upon Boron Substitution of Carbon Nanotubes. *Phys. Rev. B: Condens. Matter Mater. Phys.* **2004**, *69*, 245403.
14. Cruz-Silva, E.; López-Urias, F.; Muñoz-Sandoval, E.; Sumpter, B. G.; Terrones, H.; Charlier, J.-C.; Meunier, V.; Terrones, M. Electronic Transport and Mechanical Properties of Phosphorus- and Phosphorus-Nitrogen-Doped Carbon Nanotubes. *ACS Nano* **2009**, *3*, 1913–1921.
15. Latil, S.; Roche, S.; Mayou, D.; Charlier, J.-C. Mesoscopic Transport in Chemically Doped Carbon Nanotubes. *Phys. Rev. Lett.* **2004**, *92*, 256805.
16. Krstić, V.; Rikken, G. L. J. A.; Bernier, P.; Roth, S.; Glerup, M. Nitrogen Doping of Metallic Single-Walled Carbon Nanotubes: n-Type Conduction and Dipole Scattering. *Europhys. Lett.* **2007**, *77*, 37001.
17. Khalfoun, H.; Hermet, P.; Henrard, L.; Latil, S. B and N Co-Doping Effect in Carbon Nanotubes Electronic Transport. *Phys. Rev. B: Condens. Matter Mater. Phys.* **2010**, *81*, 193411.
18. Lherbier, A.; Blase, X.; Niquet, Y.-M.; Triozon, F.; Roche, S. Charge Transport in Chemically Doped 2D Graphene. *Phys. Rev. Lett.* **2008**, *101*, 036808.
19. Wang, X.; Li, X.; Zhang, L.; Yoon, Y.; Weber, P. K.; Wang, H.; Guo, J.; Dai, H. N-Doping of Graphene Through Electrothermal Reactions with Ammonia. *Science* **2009**, *324*, 768–771.
20. Maciel, I. O.; Anderson, N.; Pimenta, M. A.; Hartschuh, A.; Qian, H.; Terrones, M.; Terrones, H.; Campos-Delgado, J.; Rao, A. M.; Novotny, L.; *et al.* Electron and Phonon Renormalization near Charged Defects in Carbon Nanotubes. *Nat. Mater.* **2008**, *7*, 878–883.

21. Meunier, V.; Lambin, P. Tight-Binding Computation of the STM Image of Carbon Nanotubes. *Phys. Rev. Lett.* **1998**, *81*, 5588–5591.
22. Kane, C. L.; Mele, E. J. Broken Symmetries in Scanning Tunneling Images of Carbon Nanotubes. *Phys. Rev. B: Condens. Matter Mater. Phys.* **1999**, *59*, R12759–R12762.
23. Odom, T. W.; Huang, J.-L.; Kim, P.; Lieber, C. M. Atomic Structure and Electronic Properties of Single-Walled Carbon Nanotubes. *Nature* **1998**, *391*, 62–64.
24. Wildoer, J. W. G.; Venema, L. C.; Rinzler, A. G.; Smalley, R. E.; Dekker, C. Electronic Structure of Atomically Resolved Carbon Nanotubes. *Nature* **1998**, *391*, 59–61.
25. Lin, H.; Lagoute, J.; Repain, V.; Chacon, C.; Girard, Y.; Ducastelle, F.; Amara, H.; Loiseau, A.; Hermet, P.; Henrard, L.; *et al*. Imaging the Symmetry Breaking of Molecular Orbitals in Single Wall Carbon Nanotubes. *Phys. Rev. B: Condens. Matter Mater. Phys*. **2010**, *81*, 235412.
26. Hiebel, F.; Mallet, P.; Varchon, F.; Magaud, L.; Veuillen, J.-Y. Graphene-Substrate Interaction on 6H-SiC(0001): A Scanning Tunneling Microscopy Study. *Phys. Rev. B: Condens. Matter Mater. Phys.* **2008**, *78*, 153412.
27. Amara, H.; Latil, S.; Meunier, V.; Lambin, P.; Charlier, J.-C. Scanning Tunneling Microscopy Fingerprints of Point Defects in Graphene: A Theoretical Prediction. *Phys. Rev. B: Condens. Matter Mater. Phys.* **2007**, *76*, 115423.
28. Terrones, M.; Ajayan, P. M.; Banhart, F.; Blase, X.; Carroll, D. L.; Charlier, J.-C.; Czerw, R.; Foley, B.; Grobert, N.; Kamalakaran, R.; *et al*. N-Doping and Coalescence of Carbon Nanotubes: Synthesis and Electronic Properties. *Appl. Phys. A: Solids Surf.* **2002**, *74*, 355–361.
29. Czerw, R.; Terrones, M.; Charlier, J.-C.; Blase, X.; Foley, B.; Kamalakaran, R.; Grobert, N.; Terrones, H.; Tekleab, D.; Ajayan, P. M.; *et al*. Identification of Electron Donor States in N-Doped Carbon Nanotubes. *Nano Lett.* **2001**, *1*, 457–460.
30. Lin, H.; Lagoute, J.; Chacon, C.; Arenal, R.; Stéphan, O.; Repain, V.; Girard, Y.; Enouz, S.; Bresson, L.; Rousset, S.; *et al*. Combined STM/STS, TEM/EELS Investigation of CN_x-SWNTs. *Phys. Status Solidi B* **2008**, *245*, 1986–1989.
31. Czerw, R.; Chiu, P. W.; Choi, Y. M.; Lee, D. S.; Carroll, D. L.; Roth, S.; Park, Y. W. Substitutional Boron-Doping of Carbon Nanotubes. *Current Appl. Phys.* **2002**, *2*, 473–477.
32. Venema, L. C.; Meunier, V.; Lambin, P.; Dekker, C. Atomic Structure of Carbon Nanotubes from Scanning Tunneling Microscopy. *Phys. Rev. B: Condens. Matter Mater. Phys.* **2000**, *61*, 2991–2996.
33. Tománek, D.; Louie, S. G. First-Principles Calculation of Highly Asymmetric Structure in Scanning-Tunneling-Microscopy Images of Graphite. *Phys. Rev. B: Condens. Matter Mater. Phys.* **1988**, *37*, 8327–8336.
34. Stolyarova, E.; Rim, K. T.; Ryu, S.; Maultzsch, J.; Kim, P.; Brus, L. E.; Heinz, T. F.; Hybertsen, M. S.; Flynn, G. W. High-Resolution Scanning Tunneling Microscopy Imaging of Mesoscopic Graphene Sheets on an Insulating Surface. *Proc. Natl. Acad. Sci. U.S.A.* **2007**, *104*, 9209–9212.
35. Lim, S. H.; Li, R.; Ji, W.; Lin, J. Effects of Nitrogenation on Single-Walled Carbon Nanotubes within Density Functional Theory. *Phys. Rev. B: Condens. Matter Mater. Phys.* **2007**, *76*, 195406.
36. Sánchez-Portal, D.; Ordejón, P.; Artacho, E.; Soler, J. M. Density-Functional Method for Very Large Systems with LCAO Basis Sets. *Int. J. Quantum Chem.* **1997**, *65*, 453–461.
37. Perdew, J. P.; Zunger, A. Self-Interaction Correction to Density-Functional Approximations for Many-Electron Systems. *Phys. Rev. B: Condens. Matter Mater. Phys.* **1981**, *23*, 5048–5079.
38. Troullier, N.; Martins, J. L. Efficient Pseudopotentials for Plane-Wave Calculations. *Phys. Rev. B: Condens. Matter Mater. Phys.* **1991**, *43*, 1993–2006.
39. Artacho, E.; Sánchez-Portal, D.; Ordejón, P.; Garcia, A.; Soler, J. M. Linear-Scaling *ab Initio* Calculations for Large and Complex Systems. *Phys. Status Solidi B* **1999**, *215*, 809–817.
40. Monkhorst, H. J.; Pack, J. D. Special Points for Brillouin-Zone Integrations. *Phys. Rev. B: Condens. Matter Mater. Phys.* **1976**, *13*, 5188–5192.
41. Tersoff, J.; Hamann, D. R. Theory and Application for the Scanning Tunneling Microscope. *Phys. Rev. Lett.* **1983**, *50*, 1998–2001.